Article

Cell Reports

Intralymphatic CCL21 Promotes Tissue Egress of Dendritic Cells through Afferent Lymphatic Vessels

Graphical Abstract

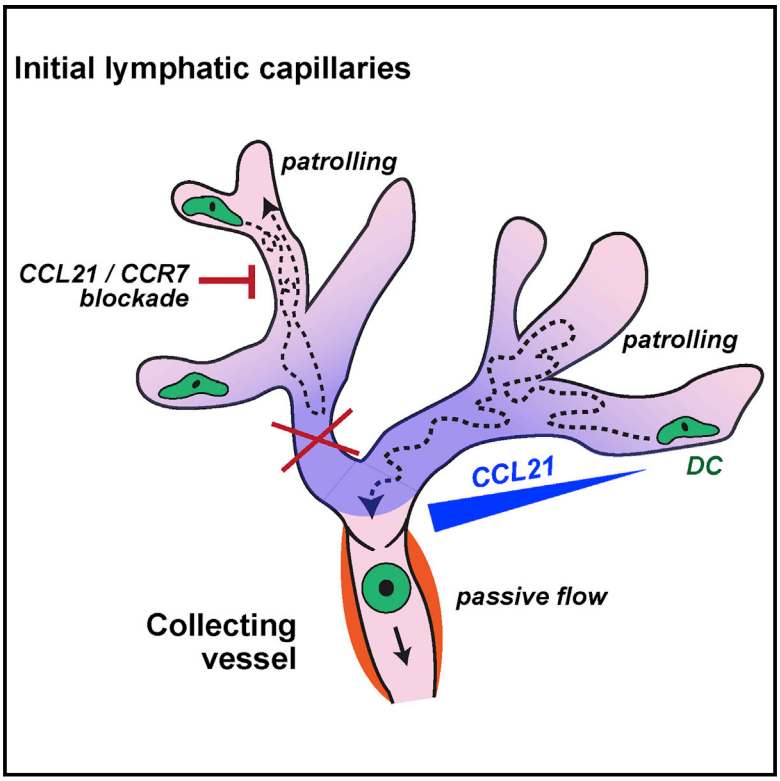

Authors

Erica Russo, Alvaro Teijeira, Kari Vaahtomeri, ..., Dontscho Kerjaschki, Michael Sixt, Cornelia Halin

Correspondence

cornelia.halin@pharma.ethz.ch

In Brief

Intravital microscopy studies have recently revealed that dendritic cells (DCs) migrating to draining lymph nodes actively crawl within afferent lymphatic capillaries. Here, Russo et al. provide evidence that an intraluminal CCL21 gradient, which is deposited by lymph flow, guides DCs migrating within capillaries in the downstream direction of the collecting lymphatic vessels.

Highlights

- Downstream-directed DC migration in lymphatic capillaries is lymph flow independent
- Downstream-directed DC migration in lymphatic capillaries is CCL21/CCR7 dependent
- Low flow creates a downstream-oriented CCL21 gradient along lymphatic endothelium
- The flow-induced CCL21 gradient promotes DC trafficking through afferent lymphatics

Russo et al., 2016, Cell Reports *14*, 1723–1734
February 23, 2016
http://dx.doi.org/10.1016/j.celrep.2016.01.048

CellPress

Cell Reports
Article

Intralymphatic CCL21 Promotes Tissue Egress of Dendritic Cells through Afferent Lymphatic Vessels

Erica Russo,[1,5] Alvaro Teijeira,[1,5] Kari Vaahtomeri,[2] Ann-Helen Willrodt,[1] Joël S. Bloch,[1] Maximilian Nitschké,[1] Laura Santambrogio,[3] Dontscho Kerjaschki,[4] Michael Sixt,[2] and Cornelia Halin[1,*]
[1]Institute of Pharmaceutical Sciences, ETH Zurich, 8093 Zurich, Switzerland
[2]IST Austria, Institute of Science and Technology Austria, 3400 Klosterneuburg, Austria
[3]Albert Einstein College of Medicine, New York, NY 10461, USA
[4]Medical University of Vienna, 1090 Vienna, Austria
[5]Co-first author
*Correspondence: cornelia.halin@pharma.ethz.ch
http://dx.doi.org/10.1016/j.celrep.2016.01.048

SUMMARY

To induce adaptive immunity, dendritic cells (DCs) migrate through afferent lymphatic vessels (LVs) to draining lymph nodes (dLNs). This process occurs in several consecutive steps. Upon entry into lymphatic capillaries, DCs first actively crawl into downstream collecting vessels. From there, they are next passively and rapidly transported to the dLN by lymph flow. Here, we describe a role for the chemokine CCL21 in intralymphatic DC crawling. Performing time-lapse imaging in murine skin, we found that blockade of CCL21—but not the absence of lymph flow—completely abolished DC migration from capillaries toward collecting vessels and reduced the ability of intralymphatic DCs to emigrate from skin. Moreover, we found that in vitro low laminar flow established a CCL21 gradient along lymphatic endothelial monolayers, thereby inducing downstream-directed DC migration. These findings reveal a role for intralymphatic CCL21 in promoting DC trafficking to dLNs, through the formation of a flow-induced gradient.

INTRODUCTION

Dendritic cell (DC) migration from peripheral tissues through afferent lymphatic vessels (LVs) to draining lymph nodes (dLNs) is essential for sustaining peripheral tolerance and for promoting immune responses against pathogens or vaccines (Förster et al., 2012; Ueno et al., 2007). Over the past 15 years, several molecular mediators of DC migration into LVs have been identified (Förster et al., 2012; Teijeira et al., 2014). Above all, the prominent role of the chemokine CCL21, which is constitutively expressed by LVs, and its DC-expressed receptor, the CC-chemokine receptor 7 (CCR7), in DC trafficking to dLNs has been recognized (Förster et al., 1999; Saeki et al., 1999). Recently, time-lapse imaging studies have provided further, cellular insights into DC migration through afferent LVs. In particular, these studies have revealed that DC trafficking through afferent LVs occurs in distinct steps. In a first step, CCR7-expressing DCs are guided toward LVs by haptotactic migration along the immobilized peri-lymphatic CCL21 gradient (Weber et al., 2013). Once in proximity of lymphatic capillaries, CCL21 also supports the docking of DCs onto lymphatic endothelial cells (LECs) (Tal et al., 2011). Subsequently, DCs enter into lymphatic capillaries by squeezing through characteristic flaps that are formed between neighboring oak-leaf-shaped LECs (Baluk et al., 2007; Pflicke and Sixt, 2009). Once within the vessels, DCs actively crawl through the capillaries (Nitschké et al., 2012; Sen et al., 2010; Tal et al., 2011). Intriguingly, DCs do not migrate completely directionally from capillaries into the downstream collecting LVs. Rather, they display a semi-directed patrolling behavior, as they frequently turn within capillaries and migrate for some time in the opposite direction of drainage (Nitschké et al., 2012; Tal et al., 2011). The final step, namely, passive transport by lymph flow, is only observed within downstream-located collecting LVs (Nitschké et al., 2012; Tal et al., 2011), likely because lymph flow in capillaries (in the order of 1–30 μm/s [Berk et al., 1996; Swartz et al., 1996]) is too low to support passive transport. Nevertheless, efficient propagation of DCs from peripheral tissues to dLNs depends on a rapid transport phase by flow, since the migratory speed of DCs within capillaries (5–8 μm/min [Nitschké et al., 2012; Tal et al., 2011]) is too slow to explain how DCs could arrive in dLNs within 6 hr to 1 day after onset of migration (Allan et al., 2006; Kissenpfennig et al., 2005). These considerations imply that active migration of DCs from lymphatic capillaries into the collecting vessels represents a rate-limiting step in the propagation of DCs to the dLN and therefore prompted us to further investigate the signals that control this process. Surprisingly, we found that DCs within lymphatic capillaries of explanted skin continued to preferentially migrate in the downstream direction, suggesting that—rather than lymph flow—chemotactic signals deposited in the vessel lumen might account for this behavior. In support of this hypothesis, we found that downstream-directed migration

of DCs within lymphatic capillaries and emigration of intralymphatic DCs through the lymphatic network was dependent on CCL21/CCR7 signaling. Moreover, in in vitro flow chamber experiments, low but not high laminar flow induced the formation of a functional CCL21 gradient along LEC monolayers, suggesting a role for lymph flow in the establishment of a haptotactic intraluminal CCL21 gradient. The latter directs active migration of DCs from capillaries toward the collecting vessels, to enable their subsequent rapid transport to the dLN by lymph flow.

RESULTS

Preferential Migration of DCs within Lymphatic Capillaries in the Downstream Direction Occurs Independently of Lymph Flow

We have recently established an intravital microscopy (IVM) model in which adoptively transferred, yellow fluorescent protein (YFP)-expressing DCs are imaged in the ear skin of VE-cadherin-Cre × RFP mice (Nitschké et al., 2012) (Figure 1A). Using this model, we observed that DCs within the capillaries migrated in a semi-directed manner toward the collecting vessels (Nitschké et al., 2012) (Movies S1, S2, and S3). To accurately quantify directedness of cell migration within LVs, we established a new parameter: the downstream migration index (DMI). The DMI is based on the optimal migratory path (OMP), the shortest path along a vessel midline that an intralymphatic DC can migrate (Figure 1B). To calculate the DMI, the OMP is divided by the total path length (TPL). Moreover, a positive or negative value is assigned to the product, depending on whether net migration occurred in the downstream or upstream direction of the LV tree, respectively (Figure 1B). In agreement with our qualitative assessment, the majority but not all adoptively transferred intralymphatic DCs displayed a positive DMI, indicating semi-directed migration (Figures 1C and 1D). Blood flow was recently shown to impact the directionality of leukocyte crawling within blood vessels (BVs) (Bartholomäus et al., 2009; Phillipson et al., 2009), but the impact of flow on the migration of intralymphatic DCs remains unclear (Nitschké et al., 2012; Tal et al., 2011). In agreement with our previous findings (Nitschké et al., 2012), injection of PBS, to experimentally increase lymph flow, did not alter the degree of downstream-directed migration (Figures 1C and 1D). To further investigate the potential contribution of flow, we performed time-lapse imaging experiments in ear skin explants that lack interstitial and intralymphatic flow. Upon addition of YFP^+ DCs to the dermal sides of ear tissue explants, many DCs were observed crawling within LVs with morphologic characteristics of capillaries (blind ends, wide, tortuous shape) but also in vessels with a collector-like morphology (thinner and more straight, presence of valves) (Figure 1E; Movies S4 and S5; Figure S1). Interestingly, even in explants DCs within vessels with capillary-like morphology continued to migrate semi-directedly in the downstream direction (Figures 1F and 1G). Conversely, in vessels with collector-like morphology, in which DCs would typically flow in vivo, the DMI was reduced to 0 (Figures 1F and 1G). These findings demonstrated that preferential downstream migration of DCs within lymphatic capillaries did not require the presence of lymph flow and indicated that this behavior might depend on chemotactic signals deposited within the capillary lumen.

CCL21 Is Present within Lymphatic Capillaries

Given the prominent role of CCL21 in DC migration into LVs (Förster et al., 1999; Saeki et al., 1999; Weber et al., 2013) and across the subcapsular sinus into LNs (Ulvmar et al., 2014), we hypothesized that this chemokine might also play a role in intralymphatic DC migration. This, however, implied that besides its reported localization to the abluminal side of LVs (Weber et al., 2013) and in large deposits within the LEC cell body (Vigl et al., 2011; Weber et al., 2013), CCL21 would also be present in the LV lumen. To investigate this, we performed high-resolution confocal imaging in ear skin whole mounts under unfixed non-permeabilizing conditions, which allowed us to only stain extracellular but not intracellular CCL21 (Weber et al., 2013). This analysis indeed detected CCL21 immunoreactivity within the lumen of lymphatic capillaries (Figures 2A and 2B). Similarly, immune-electron microscopy performed on human skin sections revealed CCL21-specific immunogold particles on the luminal surface of dermal LECs, occasionally co-localizing with podoplanin (Kerjaschki et al., 2004) (Figure 2C). Moreover, ELISA-based quantification of CCR7 ligands detected high levels of CCL21 and CCL19 in samples of human skin-draining afferent lymph, but not in corresponding plasma samples (Figure 2D). Thus, our analyses confirmed the presence of CCL21 within LVs, suggesting that this chemokine could potentially be involved in downstream-directed migration of DCs within capillaries.

Interfering with CCR7/CCL21 Signaling Reduces Downstream Migration of DCs in Lymphatic Capillaries

We therefore studied how treatment with CCL21-blocking antibody or control immunoglobulin G (IgG) affected the intralymphatic migration of adoptively transferred DCs. CCL21 blockade had no effect on the migration speed (Figure 3A) but significantly reduced the DMI and the percentage of DCs migrating in the downstream direction within capillaries (Figures 3B and 3C). We also quantified intralymphatic migration of adoptively transferred wild-type (WT) as compared to $CCR7^{-/-}$ DCs (Figures 3D–3F). $CCR7^{-/-}$ DCs have a reduced ability to enter into LVs (Tal et al., 2011; Weber et al., 2013). However, when imaging 1 hr after injection, we typically found some intralymphatic $CCR7^{-/-}$ DCs, which likely had been forced into the vessel by the injection. Similarly to CCL21 blockade, the DMI of $CCR7^{-/-}$ DCs approached a value of 0, indicative of random migration (Figures 3E and 3F). Notably, besides reducing the DMI, CCL21 blockade or loss of CCR7 signaling also significantly reduced the chemotactic index of intralymphatic DCs and also of DCs migrating in the interstitium (data not shown). To investigate whether blockade of CCL21/CCR7 signaling would similarly impact the migration of endogenous DCs within lymphatic capillaries, we performed IVM in bone marrow (BM) chimeras (CD11c-YFP → VE-cadherin-Cre × RFP). In agreement with our previous results, CCL21 blockade did not affect the speed but reduced the DMI of endogenous DCs migrating within capillaries to approximately 0 (Figures 3G–3I). Similar findings were made when performing IVM in BM chimeras or in WT mice treated with pertussis toxin,

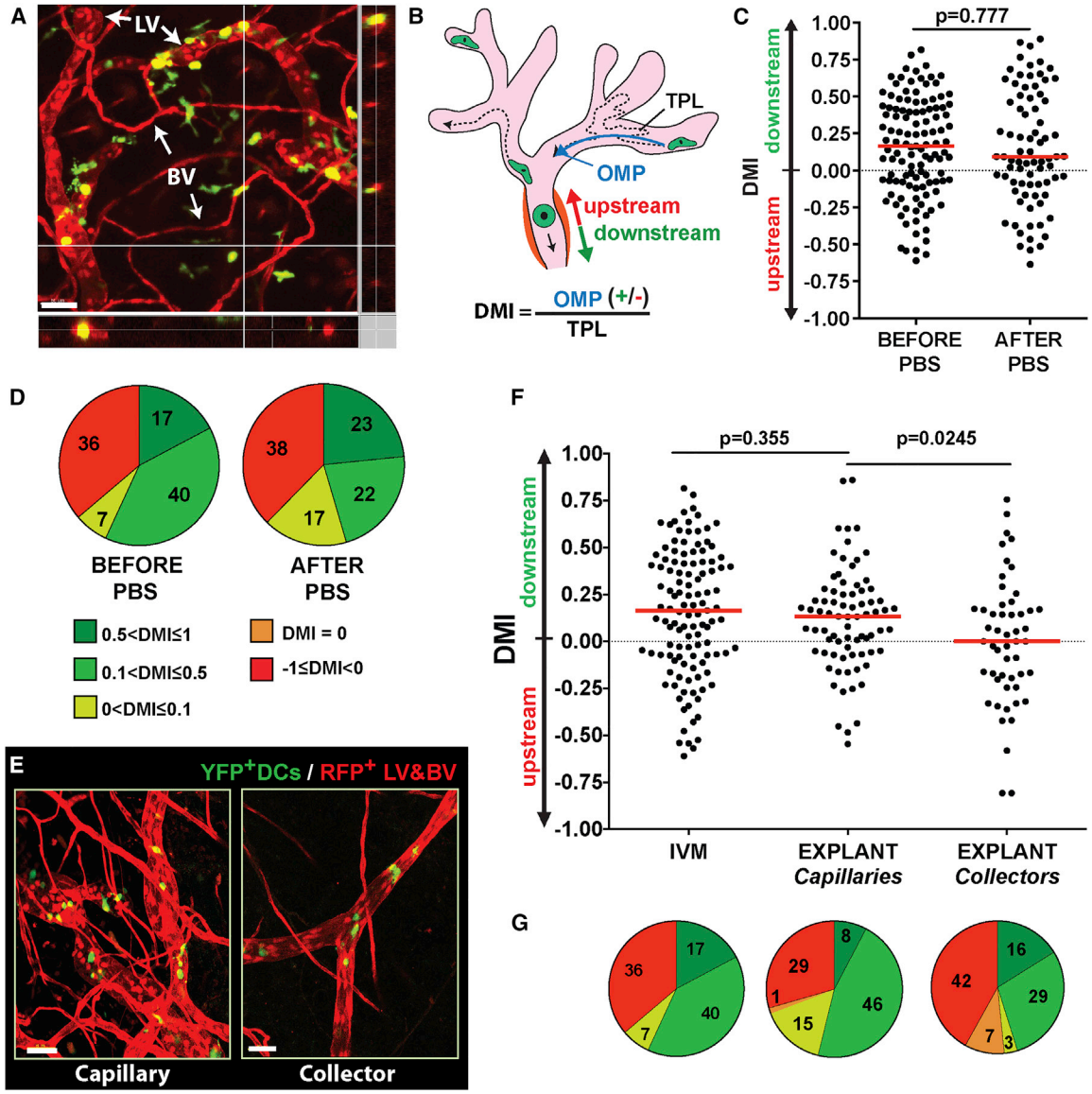

Figure 1. Preferential Migration of DCs within Lymphatic Capillaries in the Downstream Direction Occurs Independently of Lymph Flow

(A) Confocal image from an IVM experiment showing YFP$^+$ DCs patrolling within RFP$^+$ lymphatic capillaries of a VE-cadherin-Cre × RFP mouse. The latter mouse expresses red fluorescent protein (RFP) in all vessels, but LVs are easily distinguished from BVs based on morphological differences. Orthogonal views confirm the intralymphatic location of selected DCs. BV, blood vessels; LV, lymphatic vessels. Scale bar, 50 μm. Image taken from Movie S3.

(B) Graphic scheme of DCs patrolling within lymphatic capillaries or flowing in a collector. Formula for the calculation of the downstream migration index (DMI). OMP, optimal migratory path; TPL, total path length.

(C) DMI of adoptively transferred DCs migrating in lymphatic capillaries before or after PBS injection, to increase lymph flow.

(D) Color-coded percentages of DCs with positive or negative DMIs.

(E) Confocal images from ear explants of VE-cadherin-Cre × RFP mice showing YFP$^+$ DCs crawling in the lumen of LVs with capillary-like or collector-like morphology. Scale bar, 50 μm.

(F) DMI of DCs crawling in all LVs in capillary- or collector-like LVs of ear skin explants. Comparison to the DMI observed in IVM (C).

(G) Color-coded percentages of DCs with positive or negative DMIs.

Each dot in (C) and (F) represents one tracked cell. Pooled data from six (C and D) and five (F and G) different experiments per condition are shown.

which blocks Gαi-protein-coupled receptor signaling (Figure S2). To better understand why the DMI was reduced, we analyzed how the different treatment conditions affected the turning behavior of intralymphatic DCs. Blockade of CCL21/CCR7 signaling lead to intralymphatic DCs changing their migratory direction more frequently (Figure S3). In conclusion, interfering with CCL21 or CCR7 signaling reduced the ability of adoptively transferred and of endogenous intralymphatic DCs to preferentially migrate in the direction of the downstream collecting vessels.

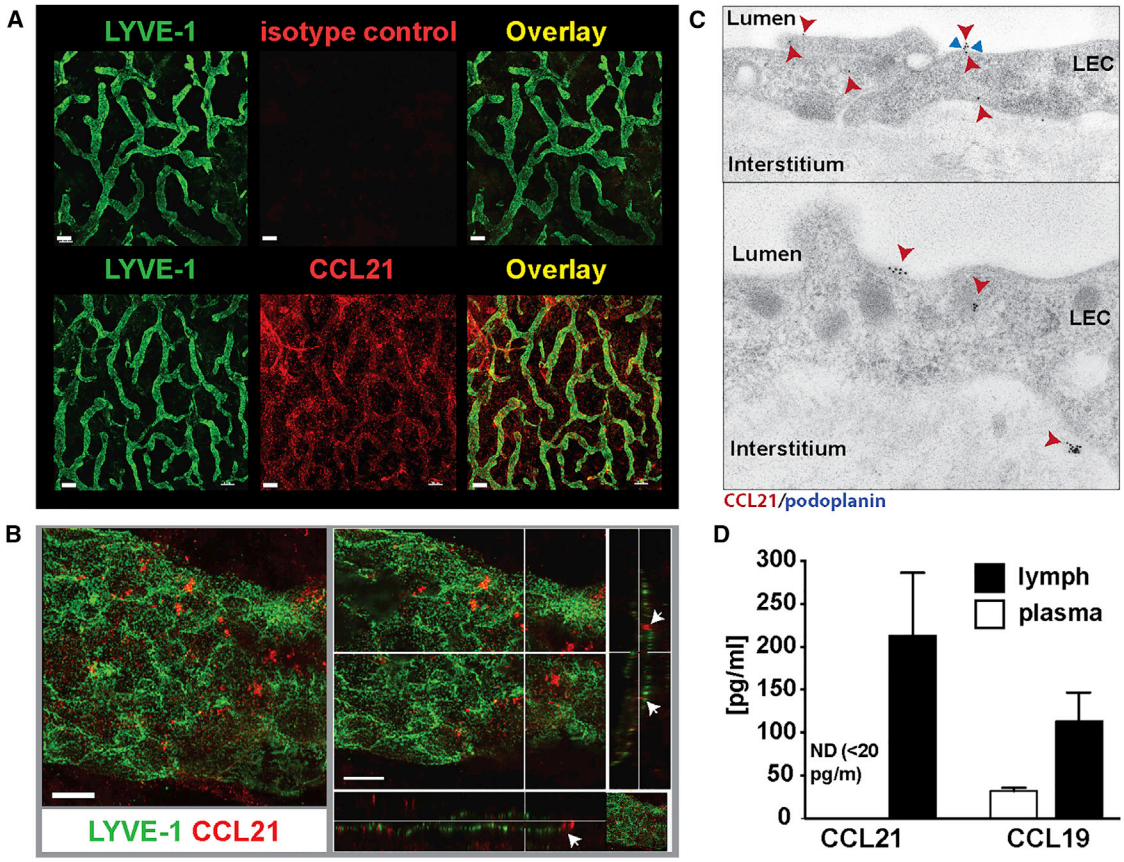

Figure 2. CCL21 Is Present within Lymphatic Capillaries

(A) Immunofluorescent whole-mount analysis of extracellular CCL21 performed in unfixed, non-permeabilized ear skin. Scale bar, 100 μm.

(B) High-magnification confocal image of CCL21 in a LYVE-1^{+} LV. Orthogonal views reveal intraluminal CCL21 (white arrows). Scale bar, 10 μm.

(C) Immunoelectron microscopic localization of CCL21 (10-nm gold particles, red arrowhead) on podoplanin-expressing (5-nm gold particles, blue arrowhead) dermal LECs in human skin sections.

(D) ELISA-based quantification of CCL19 and CCL21 in human skin-draining afferent lymph and corresponding blood plasma samples (n = 3).

Low Flow Establishes Concentrational Shifts of CCL21 along the Surface of In-Vitro-Cultured LEC Monolayers

Our findings suggested that CCL21 was present, although not homogenously distributed, in the lumen of lymphatic capillaries (Figure 2). Moreover, the overall preference of DCs to migrate in the downstream direction suggested that higher CCL21 levels might be present in the more downstream-located capillary segments. Notably, CCL21 contains a positively charged C-terminal moiety that mediates its binding to negatively charged macromolecules, such as heparan sulfates (HS) in the extracellular matrix or on cell surfaces (Bao et al., 2010; Weber et al., 2013). We therefore hypothesized that the lymph flow conditions present within lymphatic capillaries might contribute to the formation of a downstream-oriented CCL21 gradient, by promoting CCL21 dissociation from LECs in the initial capillary segments and subsequent CCL21 rebinding to LECs located further downstream (Figure S4A). To investigate and visualize the potential formation of a flow-induced CCL21 gradient, we performed in vitro experiments with conditionally immortalized murine LECs (imLECs) (Vigl et al., 2011). Since imLECs do not express CCL21(Vigl et al., 2011), we used lentiviral vectors to generate stable imLEC cell lines expressing either full-length CCL21 fused to the fluorescent protein mCherry (CCL21-mCh), a CCL21-mCherry fusion protein lacking CCL21's positively charged C terminus (CCL21ΔC-mCh), or imLECs expressing mCherry (mCh) only (Figures S4B–S4F). To investigate whether flow could establish a downstream-oriented CCL21 gradient on lymphatic endothelium, we cultured confluent monolayers of CCL21-mCh-expressing imLECs or mCh-expressing control imLECs for 24 hr in the presence of low flow (0.015 dyn/cm^2), to mimic conditions in lymphatic capillaries (Berk et al., 1996; Swartz et al., 1996). When subsequently analyzing the mCh signal, we observed that the downstream regions of flow-exposed imLEC monolayers expressing CCL21-mCH displayed overall higher mCh signals than downstream regions of control monolayers (Figures 4A and 4B). Notably, increased mCh signals in downstream regions of flow-exposed monolayers were only observed with CCL21-mCH-expressing imLECs, but not when exposing mCh-expressing control imLECs to flow (Figure S5). Overall, these findings suggested a flow-induced shift of CCL21 from upstream to downstream regions of the imLEC monolayers.

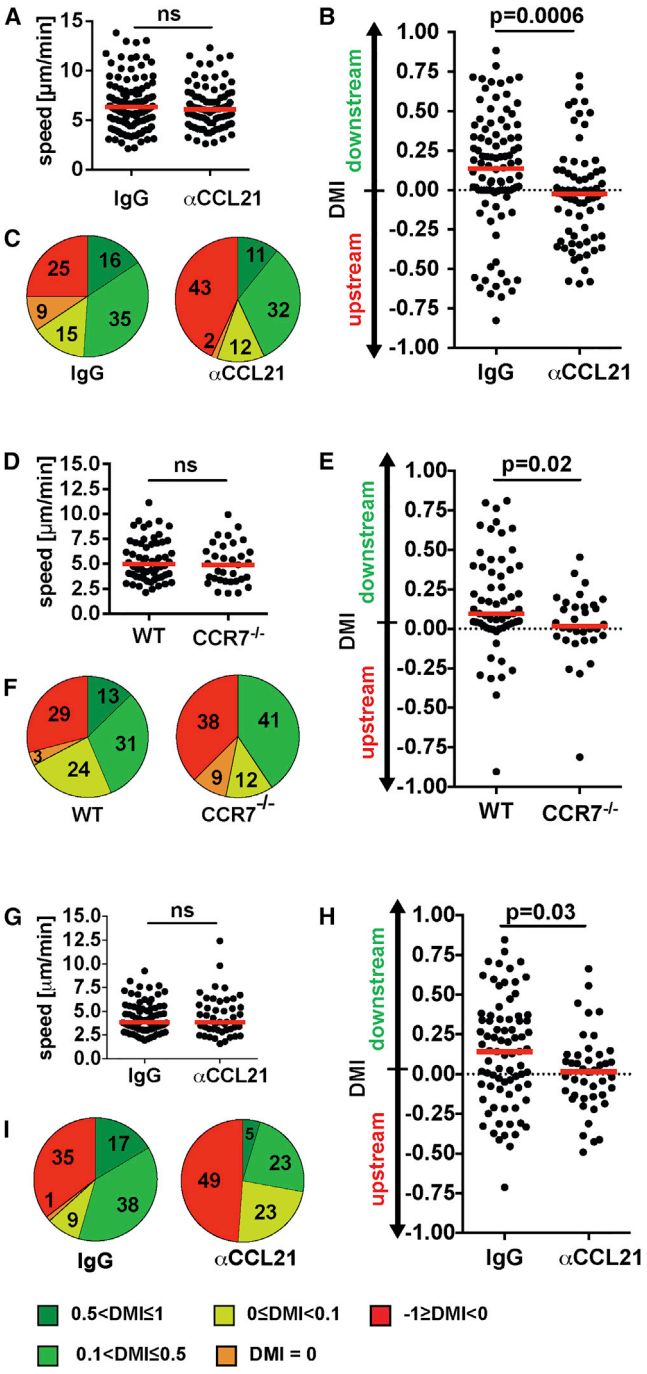

Figure 3. Interfering with CCR7/CCL21 Signaling Reduces Downstream Migration of DCs within Lymphatic Capillaries

(A–F) Analysis of the intralymphatic speed and of the DMI of adoptively transferred DCs. IVM-based quantification of DC migration within lymphatic capillaries was performed (A–C) 4 hr after adoptive DC transfer and anti-CCL21 treatment or (D–F) 1 hr after adoptive transfer of either WT or CCR7$^{-/-}$ DCs.

(G–I) Analysis of the speed and of the DMI of endogenous DCs: IVM was performed in BM chimeric VE-cadherin-Cre × RFP mice that had been reconstituted with BM of CD11c-YFP mice. Prior to IVM, DC migration was induced in the ear skin of the chimeras by topical treatment with imiquimod and intradermal injection of LPS. Each dot represents one tracked cell. Pooled data from six to nine different experiments per condition are shown.

(C, F, and I) Color-coded percentages of DCs with positive or negative DMIs.

Low Flow Generates a Functional CCL21 Gradient along the Surface of In-Vitro-Cultured LEC Monolayers

We next performed time-lapse imaging of DCs placed onto flow-exposed or resting (no flow) imLECs, to investigate whether pre-exposure to flow was capable of establishing a functional CCL21 gradient along imLECs monolayers. To quantify DC directionality in the flow chamber setup, we devised a new parameter: the in vitro DMI (*iv*DMI) is calculated by dividing the x axis component of the cellular displacement by the TPL. In analogy to the DMI, the *iv*DMI is assigned a positive or negative value, depending on which direction (i.e., with or against the applied flow) the cell had migrated (Figure 4C). For DC migration experiments, the three different imLEC cell lines were cultured for 24 hr in the presence or absence of flow. DCs were subsequently added onto the monolayers and their migration recorded in the absence of flow. Analysis of the cell migration tracks revealed that DCs placed onto flow-exposed CCL21-mCh-expressing monolayers indeed displayed preferential migration in the downstream direction of flow (Figures 4D and 4E). By contrast, no downstream-directed migration was observed on CCL21-mCh-expressing monolayers cultured in the absence of flow, or when DCs were placed onto flow-exposed monolayers expressing mCh only or CCL21ΔC-mCh lacking the positively charged, LEC-binding C terminus (Figures 4D and 4E). Similarly, when imaging the migration of WT and CCR7$^{-/-}$ DCs on imLEC monolayers expressing CCL21-mCh, preferential migration in the downstream direction was only observed in WT but not in CCR7$^{-/-}$ DCs migrating on flow-exposed imLECs (Figures 4F and 4G). In conclusion, flow-induced preferential migration in the downstream direction was mediated by CCL21 and required the immobilization of CCL21 on the imLEC cell surface.

The Formation of a Functional CCL21 Is Shear Rate Dependent

Intriguingly, we observed that the ability of flow to establish a haptotactic CCL21 gradient along imLEC monolayers was dependent on the shear strength applied: when performing DC migration experiments on CCL21-mCh imLECs that had been exposed to 100-fold higher shear rates (1.5 dyn/cm^2), to mimic shear rate conditions in BVs or in contracting lymphatic collectors, preferential migration in the downstream direction of flow was completely abolished (Figures 5A and 5B).

Immobilized CCL21 Accounts for Downstream Migration in Capillaries of Skin Explants

With these results, we went back to the ear explant model to investigate whether also in this setup, in absence of flow, DC migration in the downstream direction was dependent on CCL21/CCR7 signaling. Performing experiments with fluorescently labeled CCR7$^{-/-}$ DCs, we observed that cell entry into LVs was reduced, albeit still sufficient to analyze intralymphatic behavior of CCR7$^{-/-}$ cells. Similarly to the in vivo situation, we observed that only WT but not CCR7$^{-/-}$ DCs preferentially migrated in the downstream direction in vessels with

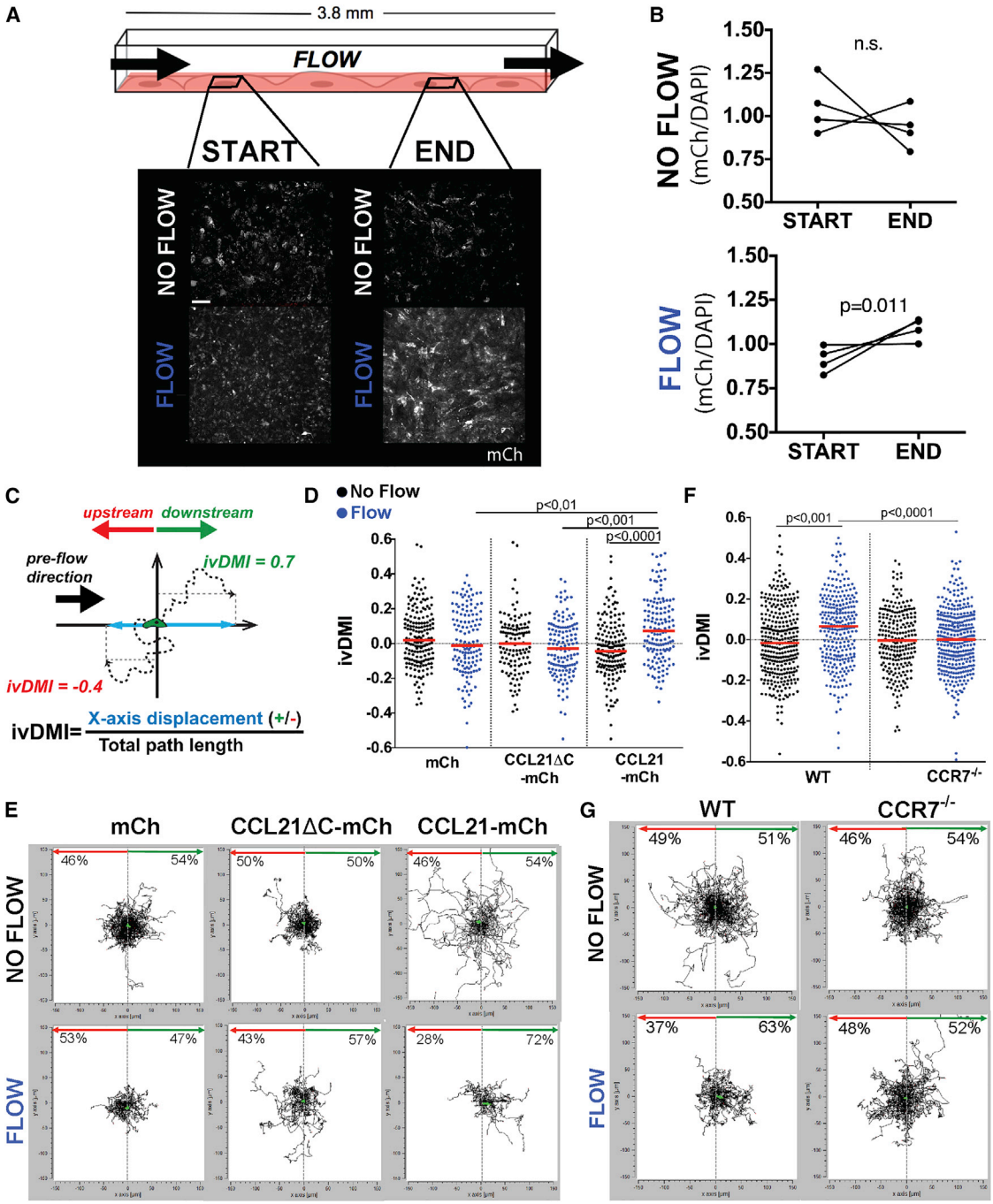

Figure 4. Flow Generates a Functional CCL21 Gradient on the Surface of In-Vitro-Cultured Murine LECs

(A and B) CCL21-mCh expressing imLEC monolayers were cultured 24 hr in absence (NO FLOW) or presence of low laminar flow (FLOW – 0.015 dyn/cm^2). mCh and DAPI intensities were measured in two defined regions of the chamber. (A) Illustration of the experiment and representative images of the mCh signal (white). (B) Quantification of mCh signal, normalized to DAPI (to account for potential differences in cell numbers) (n = 4 experiments).

(C) Schematic and mathematical explanation of the in vitro *DMI*.

(D) *iv*DMI of DCs crawling on flow-exposed or control-treated imLEC monolayers expressing mCh, CCL21-mCh, and CCL21ΔC-mCh.

(F) *iv*DMI of fluorescently labeled WT as compared to CCR7$^{-/-}$ DCs crawling on flow-exposed (FLOW) or control (NO FLOW) imLEC monolayers expressing CCL21-mCh. Each dot represents one tracked cell. Pooled data from three different experiments per condition are shown.

(E and G) Track plots from one out of three similar experiments. The central light green arrow indicates the overall migration directionality and represents the sum of the displacement vectors of all tracked cells. The percentages of cells migrating in downstream or upstream direction are indicated below the horizontal green or red arrows at the top.

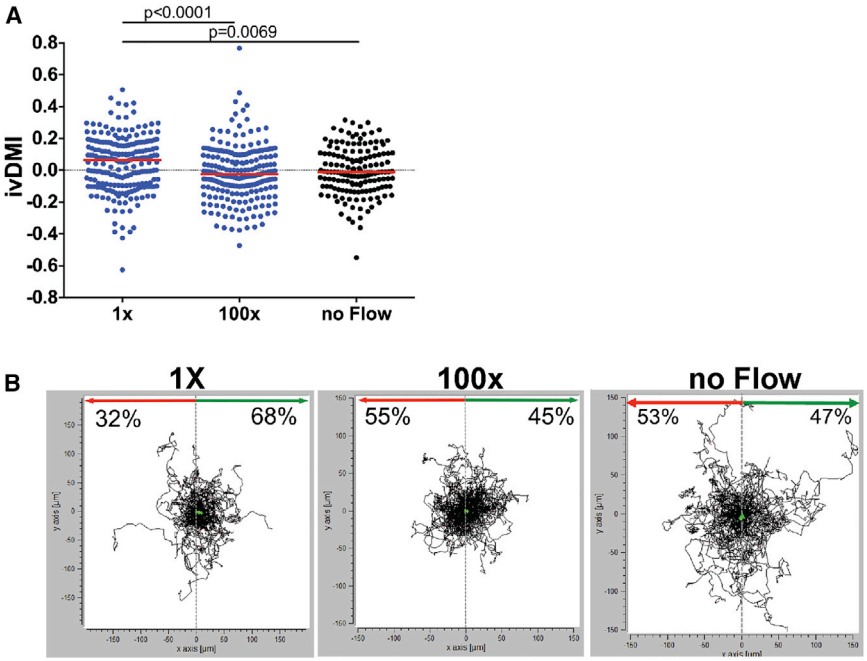

Figure 5. A Functional CCL21 Gradient Formation Is Induced under Low-Flow but Not under High-Flow Conditions

CCL21-mCh expressing imLEC monolayers were cultured 24 hr in absence (CONTROL) or presence of low (0.015 dyn/cm^2 – 1×) or high (1.5 dyn/cm^2 – 100×) laminar flow, to mimic conditions in lymphatic capillaries and blood vessels, respectively. Subsequently, migration of YFP$^+$ DCs was quantified by performing time-lapse imaging experiments.

(A) Analysis of the *iv*DMI. Each dot represents one tracked cell. Pooled data from three different experiments per condition are shown.

(B) Track plots from one out of three similar experiments. In each plot, the central light green arrow indicates the overall migration directionality and represents the sum of the displacement vectors of all tracked cells. The percentages of cells displaying overall migration in downstream or upstream direction is indicated below the horizontal green or red arrows at the top.

capillary-like morphology (Figures 6A and 6B). Neither WT nor CCR7$^{-/-}$ DCs migrated directedly in vessels with a collector-like phenotype (Figures 6A and 6B), in agreement with our observation that CCL21 expression was reduced or absent in lymphatic collectors (Figure S5). Overall, our findings confirmed that CCR7 signaling but not lymph flow was responsible for downstream migration of DCs within lymphatic capillaries.

Our in vitro flow chamber data had indicated that CCL21 needed to be immobilized on LECs via its positively charged C terminus in order to mediate flow-induced downstream migration of DCs (Figures 4D and 4E). Since HS was previously shown to account for the immobilization of CCL21 on and around LECs (Bao et al., 2010; Weber et al., 2013; Yin et al., 2014), we investigated its involvement in intralymphatic DC migration. Therefore, we imaged DC migration within capillaries of ear explants that had been pre-treated with heparitinases, thereby abolishing co-localization of CCL21 with LVs (Weber et al., 2013) (Figure 6C). Pre-treatment with heparitinases significantly reduced the DMI, and the percentage of DCs migrating in the downstream direction within capillary-like vessels of ear explants (Figures 6D and 6E). These findings indicated that HS was important for immobilization of CCL21 on the luminal side of lymphatic capillaries and for the establishment of the intraluminal gradient.

CCL21 Blockade Reduces Emigration of Intralymphatic DCs from the Skin

We next investigated whether, besides reducing the DMI of intralymphatic DCs (Figure 3), blockade of CCL21 would also affect the overall ability of DCs within lymphatic capillaries to advance through afferent LVs. We addressed this in the ear explant setting, where we first allowed lipopolysaccharide (LPS)-matured YFP$^+$ DCs to migrate for 4 hr into the dermis and into lymphatic capillaries. At this time point, 89% of all DCs within the explant were present within lymphatic capillaries, with only few DCs (11%) remaining in the interstitial tissue (Figures 7A and 7B). Next, explants were treated with control- or CCL21-blocking antibodies. When imaging 4 hr later (i.e., 8 hr after starting the experiment), the percentage of lymphatic capillary area covered by DCs was significantly reduced in the control group but not in the CCL21-blocked setup, indicating that CCL21 blockade had interfered with the DCs' ability to advance from the capillaries into the collecting vessels (Figures 7C and 7D). Previous studies have shown that the emigration of DCs out of skin explants occurs through LVs (Gunn et al., 1999; Lukas et al., 1996; Stoitzner et al., 1999). In a final experiment, we therefore investigated whether blockade of CCL21 would also impair intralymphatic DCs in their overall ability to emigrate through the lymphatic network into the culture medium. For this, we again allowed YFP$^+$ DCs to enter for 4 hr into lymphatic capillaries of ear skin explants, to achieve a starting condition with approximately 90% of all YFP$^+$ DCs within lymphatic capillaries (Figures 7A and 7B). Explants were then incubated in fresh medium containing either control or CCL21-blocking antibodies and the number of DCs that had emigrated into the culture medium was determined 24 hr later. This fluorescence-activated cell sorting (FACS)-based quantification detected a significant reduction (−30%, $p = 0.0014$) in the number of DCs that had emigrated from anti-CCL21-treated as compared to control-treated explants (Figures 7E and 7F). Notably, confocal microscopy confirmed that under both treatment conditions DCs remaining in the explants at the 24-hr time point continued to mainly localize within LVs, indicating that DC emigration had primarily occurred via the lymphatic route (Figure 7G). Thus, blockade of CCL21 had reduced the ability of intralymphatic DCs to emigrate out of the explanted skin through the lymphatic network.

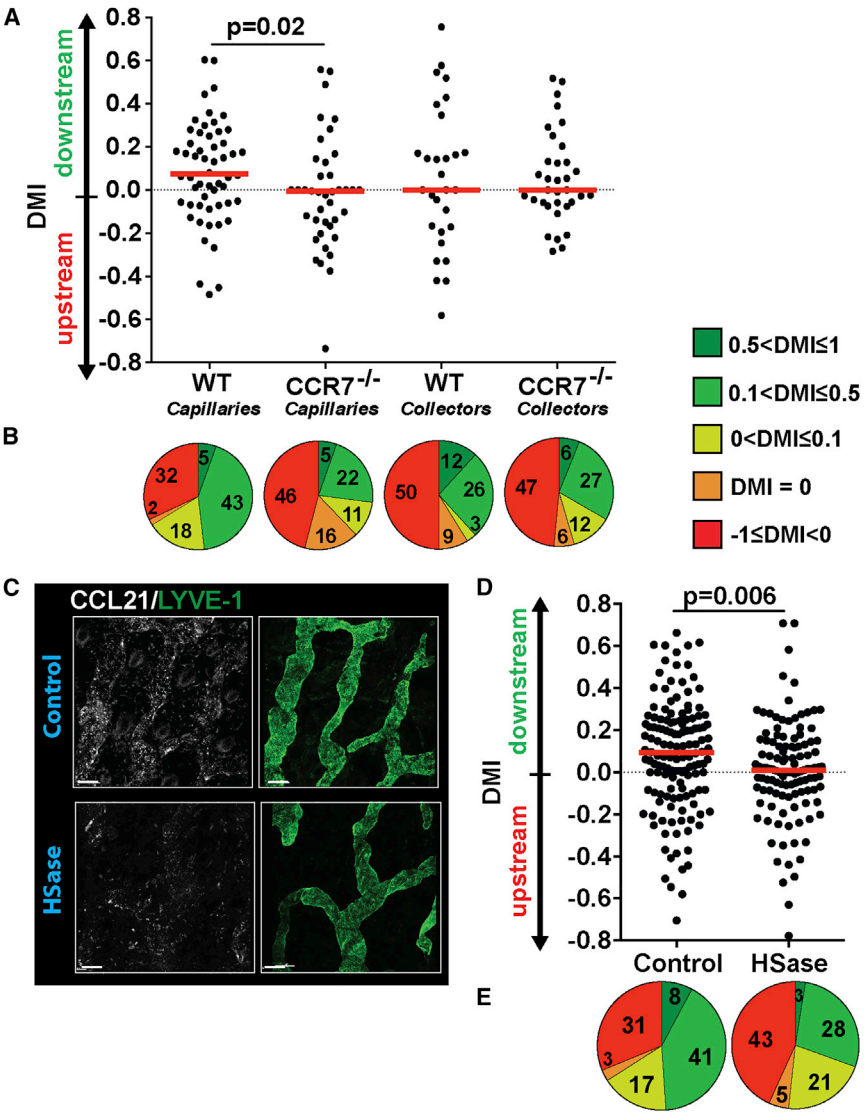

Figure 6. CCL21/CCR7 Signaling Accounts for Downstream Migration of DCs in Ear Explants

(A and B) Analysis of WT or CCR7$^{-/-}$ DCs crawling in capillary- or collector-like LVs of ear skin explants. Analysis of the (A) DMI and (B) color-coded percentages of DCs with positive or negative DMIs.

(C–E) Impact of heparitinase (HSase) treatment or treatment with control medium on DC migration within capillaries of ear explants.

(C) Effect of heparitinase treatment on colocalization of extracellular CCL21 with LYVE-1^{+} LVs. Scale bars, 50 μm.

(D and E) Effect of pre-treatment of ear tissue with heparitinase on the (D) DMI and (E) color-coded percentages of DCs with positive or negative DMIs.

Each dot in (A) and (D) represents one tracked cell. Pooled data from five different experiments per condition are shown (A and B, D and E).

DISCUSSION

CCL21/CCR7 is widely recognized as the most important driver of DC trafficking from peripheral tissues to dLNs (Förster et al., 1999; Moussion and Girard, 2011; Ulvmar et al., 2014; Weber et al., 2013). The profound impact of CCL21 on DC migration has thus far mainly been attributed to its role in DC chemotaxis toward LVs. However, CCL21 was recently shown to also mediate subsequent steps in DC migration, such as the docking and transmigration across the lymphatic endothelium as well as DC transit across the LN subcapsular sinus (Johnson and Jackson, 2010; Tal et al., 2011; Ulvmar et al., 2014), indicating a more complex role of this chemokine in lymphatic migration. In this study, we report on yet another, rather unexpected mechanism by which CCL21 promotes DC trafficking: it guides intralymphatic DCs from capillaries into collecting vessels and thereby enables them to more efficiently advance through the lymphatic network.

Leukocyte crawling in lymphatic capillaries was only recently discovered (Nitschké et al., 2012; Sen et al., 2010; Tal et al., 2011), but leukocyte crawling in BVs has been described and investigated for much longer (Bartholomäus et al., 2009; Geissmann et al., 2005; Phillipson et al., 2006, 2009). While some of the latter studies demonstrated a link between blood flow and the direction sensing of intravascular leukocytes (Bartholomäus et al., 2009; Phillipson et al., 2009), our time-lapse imaging experiments in mice and skin explants did not reveal any connection between the crawling directionality of intralymphatic DCs and lymph flow directionality. These findings were in agreement with our previous studies (Nitschké et al., 2012) but in apparent conflict with another publication, in which intradermal injection of PBS to experimentally increase lymph flow-induced DCs to migrate more directedly, i.e., with a higher chemotactic index, within LVs (Tal et al., 2011). However, since the latter study did not evaluate whether directed migration was more pronounced in the upstream or in the downstream direction, it is hard to compare these results to the ones obtained in our study. On the other hand, our findings demonstrate a strong dependence of downstream-directed migration on the DC's ability to sense CCL21. At the same time, our flow chamber findings indicated a role for lymph flow in establishing an intralymphatic CCL21 gradient. Thus, although flow is not directly affecting DC migration our data suggest that it *indirectly* guides downstream-directed migration, by contributing to the establishment of an intraluminal CCL21 gradient.

Experimental flow measurements in LVs have indicated values ranging from 1 to 30 μm/s in capillaries (Berk et al., 1996; Swartz et al., 1996), whereas in large collectors peak velocities of

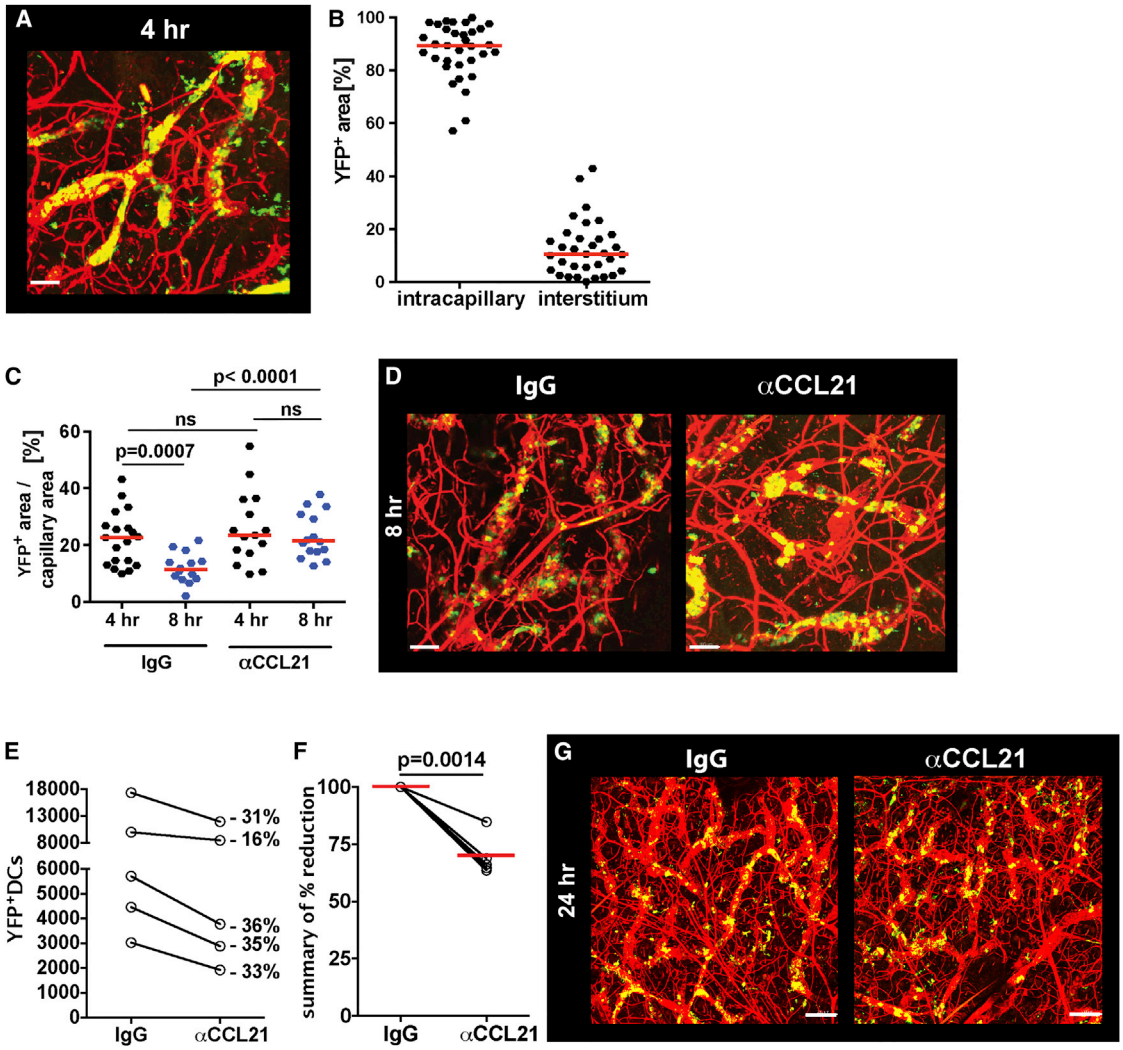

Figure 7. Blockade of CCL21 Prevents Emigration of Intralymphatic DCs from Ear Skin Explants

(A and B) YFP$^+$ LPS-matured DCs were added onto the dermal aspects of ear skin explants of VE-cadherin-Cre × RFP mice, and their localization in the tissue and within lymphatic capillaries was analyzed 4 hr later. (A) Representative confocal image of DCs within RFP$^+$ capillaries. Scale bar, 100 μm. (B) Image-based quantification of DCs within lymphatic capillaries and in the interstitium. Each dot represents one analyzed image. Pooled data from three similar experiments are shown.

(C) Quantification of DCs in lymphatic capillaries at the 4-hr time point (4 hr) and after an additional 4 hr in presence of CCL21-blocking or control antibodies (8 hr).

(D) Each dot represents quantification of one field of view. Pooled data from three experiments are shown. Representative images taken at the 8-hr time point, i.e., 4 hr after addition of antibodies. Scale bar, 100 μm.

(E and F) YFP$^+$ LPS-matured DCs were added onto the dermal aspects of ear skin explants and left to enter into LVs for 4 hr (as in A and B). Subsequently, explants were incubated in media in presence of CCL21-blocking or control antibody, and the number of DCs that had emigrated into the medium was quantified 24 hr later by FACS. (E) Quantification of DCs in five individual experiments (connected by a line). Each experiment involved two to three explants/condition. (F) Summary of the percentage reduction between control (100%) and CCL21-treated conditions in all experiments performed (n = 5).

(G) Representative images taken at the 24-hr time point. Scale bar, 200 μm.

several millimeters per minute have been recorded (Dixon et al., 2005). These measurements suggest that flow velocities and shear rates in lymphatic capillaries are two to three orders of magnitude lower than in postcapillary venules or in liver sinusoids, where intravascular leukocyte crawling has previously been observed (Bartholomäus et al., 2009; Geissmann et al., 2005; Phillipson et al., 2006). Interestingly, in our in vitro flow chamber experiments CCL21 only established a functional, downstream-oriented gradient under low flow conditions (0.015 dyn/cm^2, corresponding to approximately 8 μm/s). Downstream-directed migration was completely abolished when CCL21-mCh expressing imLEC monolayers had been precultured in presence of a 100-fold higher shear rate (1.5 dyn/cm^2), which more mimicked the flow conditions in BV capillaries or peak flow conditions in lymphatic collectors. Thus, it is possible that the high shear rates present in BVs or in lymphatic

collectors would not allow for the rebinding of chemokine in downstream vessel segments and therefore not support the establishment of a downstream-oriented intravascular gradient. Overall, our findings suggest that the low flow present in lymphatic capillaries and the constitutive expression of CCL21 by capillary LECs provide unique conditions that enable the formation of a downstream-oriented gradient. Surprisingly, we were not able to overwhelm the intralymphatic CCL21 gradient when experimentally flooding the tissue with exogenous CCL21: neither in the in vivo setup nor in ear skin explants did administration/pretreatment with recombinant CCL21 lead to a reduction in the DMI or in the chemotactic index of intralymphatic DCs (data not shown). However, we cannot exclude that this failure to overwhelm the gradient was due to experimental difficulties related to the chemokine dose or diffusion into the vessel lumen.

Visualizing the intraluminal CCL21 gradient in vivo unfortunately proved difficult, due to the strong CCL21 signal on the abluminal aspect of the vessels and the rather weak and patchy intraluminal signal. Interestingly, the staining performed on imLEC monolayers also revealed a patchy distribution pattern of CCL21 on the monolayer surface. Given our in vivo and in vitro observations, it is perceivable that the presumed intravascular CCL21 gradient within lymphatic capillaries is rather heterogeneous. This could explain why DC migration in capillaries occurs semi-directedly and involves frequent directional turns. In fact, under all conditions investigated our DMI analyses revealed that the downstream-directed component of intralymphatic DC migration only corresponded to approximately 15%–20% of the overall cellular movement; i.e., DMIs typically ranged from 0.15 to 0.2. Yet blockade of CCL21 or loss of CCR7 resulted in a complete loss of DC directionality within lymphatic capillaries (i.e., DMIs approaching a value of 0). Moreover, CCL21 blockade functionally affected the ability of DCs to emigrate from capillaries and out of the skin through the dermal lymphatic network. Thus, although intralymphatic migration in lymphatic capillaries occurs in a semi-directed manner, this directional component is crucial for the overall ability of DCs to advance through the lymphatic network.

Interestingly, studies performed more than 15–20 years ago in human or murine skin explants already reported that upon explant culture endogenous DCs accumulated in LVs and emigrated out of the skin through the lymphatic network (Gunn et al., 1999; Lukas et al., 1996; Stoitzner et al., 1999). Our findings explain how CCL21 contributes to advancing DCs through capillaries in this setup. However, it might seem puzzling that DCs in explanted skin even manage to advance through collectors, in which we found DC migration to occur completely randomly. This might be explained by the fact that in our imaging experiments the DMI of DCs migrating in collectors was typically only analyzed in the inter-valve segments, the so-called lymphangions. Although we frequently observed DCs passing through valves in the downstream direction, this passage was only rarely observed in the opposite, retrograde direction (data not shown). Thus, in the explant setting, the presence of downstream-oriented valves likely added an additional level of directedness to DC migration through collectors. In vivo, in presence of flow, the contribution of valves to directedness of passive DC movement through collectors is expected to be even more profound: in the living animal, lymphatic valves prevent fluid backflow and thus enable the efficient transport of lymph-borne leukocytes from one contracting lymphangion to the next (Dixon et al., 2005).

Although our findings strongly suggest a role for flow in the establishment of the CCL21 gradient present within lymphatic capillaries, we cannot exclude that other factors might contribute to this process. For example, it could be that CCL21 protein expression differences exist in lymphatic capillaries, with LECs located more distantly from the blind ends producing or secreting higher CCL21 levels. Interestingly, it has recently been shown that DCs can proteolytically cleave off the positively charged C terminus of CCL21 and convert it from a surface-bound to a soluble form (Schumann et al., 2010). Given that DC entry primarily occurs in the initial capillaries (Pflicke and Sixt, 2009) it is perceivable that transmigrating DCs cleaving off CCL21 from the LEC surface could preferentially reduce CCL21 levels in the capillary tip regions, thereby creating a local chemokine sink. Moreover, it is possible that local differences in the expression or intraluminal localization of macromolecules involved in CCL21 presentation, such as HS (Bao et al., 2010; Weber et al., 2013; Yin et al., 2014) or podoplanin (Kerjaschki et al., 2004), could contribute to the establishment of an intralymphatic gradient.

An unresolved question remaining is why DCs that have arrived in collecting vessels do not continue to crawl but detach to be transported by flow. Most likely, the increased flow in collecting LVs generates hydrodynamic forces that no longer support intraluminal crawling. Moreover, in agreement with a previous study in human skin (Wick et al., 2008), our FACS and immunofluorescence analyses revealed lower levels of CCL21 in collector LECs (colLECs) as compared to capillary LECs (capLECs), that might facilitate detachment of DCs from the colLEC surface and transition to a flowing mode. In the future, it will be interesting to investigate whether CCL21 also accounts for the capillary-to-collector transit of other lymph-borne leukocyte subsets that reportedly depend on CCR7 for migration to dLNs (Bromley et al., 2005, 2013; Debes et al., 2005; Menning et al., 2007).

In conclusion, our results identify CCL21 as the key molecule orchestrating intralymphatic DC migration from capillaries to collectors. Ultimately, this level of molecular and cellular insight into the process of DC migration could be of therapeutic relevance, for example, in the context of DC-based vaccines, where promotion of CCR7 signaling is expected to increase the arrival of intralymphatic DCs in the dLNs and thus the induction of adaptive immunity.

EXPERIMENTAL PROCEDURES

Mouse Strains

Wild-type (WT) C57BL/6 mice were purchased from Janvier. CCR7$^{-/-}$ (Förster et al., 1999) and CD11c-YFP mice (Lindquist et al., 2004) were bred in our facility. VE-cadherin-Cre × RFP were generated as described (Luche et al., 2007; Nitschké et al., 2012). All experiments were approved by the Cantonal Veterinary Office Zurich.

Generation of Bone Marrow-Derived DCs

BM-DCs were generated from CD11c-YFP, WT, or CCR7$^{-/-}$ mice by incubation of BM cells in granulocyte-macrophage colony-stimulating factor (GM-CSF)-containing medium (see Supplemental Experimental Procedures) (Nitschké et al., 2012).

Time-Lapse Imaging

For IVM, 0.5–1 × 10^6 LPS-activated BM-DCs in 10 μl of media were injected into two to three regions in the ventral side of the mouse ear pinna of isoflurane-anesthetized VE-Cadherin Cre × RFP mice, as previously described (Nitschké et al., 2012). IVM was started 1–3 hr after injection. Alternatively, IVM was performed in BM chimeras, i.e., VE-Cadherin-Cre × RFP mice reconstituted with BM from CD11c-YFP mice (Nitschké et al., 2012). Ex vivo imaging was performed in ear skin explants of VE-Cadherin Cre × RFP mice following a protocol established in analogy to previous reports (Pflicke and Sixt, 2009; Weber et al., 2013). Briefly, the dermal side of the explant was incubated for 30 min at 37°C with fluorescent BM-DCs in media. DCs that had not entered into the dermis were subsequently washed off, and the explant was incubated for additional 2 hr in fresh media. Imaging (IVM or explants) was performed on a Zeiss LSM 710 inverted confocal microscope (Carl Zeiss), recording time-lapse videos of 1 hr. At the end of all experiments, a tile scan of the lymphatic vasculature surrounding the imaged area was recorded, to provide information about the lymphatic network architecture and the assumed direction of drainage. All treatment protocols, imaging time points, and microscopy specifications are provided as Supplemental Experimental Procedures.

Emigration Experiments in Ear Skin Explants

See Supplemental Experimental Procedures.

Analysis of DC Motility

Videos were analyzed with IMARIS software (v.7.1.1, Bitplane). For semi-automated cell tracking, tracks were generated by an automatic algorithm and verified manually. Only tracks of cells recorded for >20 min and with a total path length of >100 μm were included in the analysis. If a cell was arrested >30 min at the beginning or at the end of its track, only the motile part of the track was evaluated. If a cell stopped >30 min in the middle of its track, it was excluded from the analysis. The same parameters were applied to the tracking of cells in in vitro experiments. To calculate the downstream migration index (DMI), a combined algorithm for digitization of cell tracks and vessels using FIJI (ImageJ) and IMARIS was developed (see Supplemental Experimental Procedures). Briefly, the algorithm generated a virtual track in the mid-line of the LV, from which the optimal migratory path (OMP) was computed. The DMI was obtained by dividing the OMP by the total path length the cell had migrated. A positive or a negative value was subsequently manually assigned to the DMI, depending on whether DC migration had occurred in the downstream or upstream direction of the LV tree, as judged from the tile scan analysis (see Supplemental Experimental Procedures). The DMI analysis was performed in a blinded manner and offline, at the end of the experiment. In cases where the direction of drainage could not be deducted form the tile scan, cells were excluded from the DMI analysis. Similarly, the morphology-based assignment of vessels into capillary-or collector-like morphology was performed offline and in a blinded fashion.

imLECs Culture, Viral Transduction, and Flow Chamber Experiments

Conditionally immortalized LECs (imLECs), expressing a heat-labile version of the large T antigen, were isolated from the back skin of H-2Kb-tsA58 (immorto) mice (Jat et al., 1991) as previously described (Vigl et al., 2011). Cell culture conditions, the generation of stable imLEC transfectants expressing mCherry (mCh), CCL21ΔC-mCh, or CCL21-mCh as well as the flow chamber experiments performed are described in the Supplemental Experimental Procedures.

Statistical Analysis

Results are presented as medians. Datasets were analyzed using the Mann-Whitney test. Differences were considered statistically significant when $p < 0.05$. Significant outliers, identified by Grubb's test, were excluded. Statistical analysis was performed with Prism 6 (GraphPad).

SUPPLEMENTAL INFORMATION

Supplemental Information includes Supplemental Experimental Procedures, six figures, and five movies and can be found with this article online at http://dx.doi.org/10.1016/j.celrep.2016.01.048.

AUTHOR CONTRIBUTIONS

E.R. and A.T. designed research, performed research, analyzed data, and wrote the paper. A.-H.W., K.V., J.S.B., M.N., and D.K. performed research and analyzed data. L.S. and M.S. provided essential reagents and discussed data. C.H. designed research, analyzed data, and wrote the paper.

ACKNOWLEDGMENTS

The authors acknowledge support of the Scientific Center for Optical and Electron Microscopy (ScopeM) of ETH Zurich, in particular, the help of Szymon Stoma and Simon Nørrelykke. We thank Simone Haener, Nicole Stoffel, Angela Landtwing, and Jasmine Frei (ETH Zurich) for excellent technical assistance and the staff of the ETH Rodent Center HCI for animal husbandry. Moreover, we thank Viola Vogel and Ima Avalos (ETH Zurich) for providing microscope access and precious assistance with flow chamber experiments. The Heisenberg lab (IST Austria), Alexandre Angers-Loustau (University of Helsinki), and the Functional Genomics unit (University of Helsinki) are acknowledged for reagents and protocols. C.H. gratefully acknowledges financial support from the Swiss National Fund (grants 310030_138330 and 310030_156269).

Received: August 19, 2015
Revised: December 4, 2015
Accepted: January 13, 2016
Published: February 11, 2016

REFERENCES

Allan, R.S., Waithman, J., Bedoui, S., Jones, C.M., Villadangos, J.A., Zhan, Y., Lew, A.M., Shortman, K., Heath, W.R., and Carbone, F.R. (2006). Migratory dendritic cells transfer antigen to a lymph node-resident dendritic cell population for efficient CTL priming. Immunity *25*, 153–162.

Baluk, P., Fuxe, J., Hashizume, H., Romano, T., Lashnits, E., Butz, S., Vestweber, D., Corada, M., Molendini, C., Dejana, E., and McDonald, D.M. (2007). Functionally specialized junctions between endothelial cells of lymphatic vessels. J. Exp. Med. *204*, 2349–2362.

Bao, X., Moseman, E.A., Saito, H., Petryniak, B., Thiriot, A., Hatakeyama, S., Ito, Y., Kawashima, H., Yamaguchi, Y., Lowe, J.B., et al. (2010). Endothelial heparan sulfate controls chemokine presentation in recruitment of lymphocytes and dendritic cells to lymph nodes. Immunity *33*, 817–829.

Bartholomäus, I., Kawakami, N., Odoardi, F., Schläger, C., Miljkovic, D., Ellwart, J.W., Klinkert, W.E., Flügel-Koch, C., Issekutz, T.B., Wekerle, H., and Flügel, A. (2009). Effector T cell interactions with meningeal vascular structures in nascent autoimmune CNS lesions. Nature *462*, 94–98.

Berk, D.A., Swartz, M.A., Leu, A.J., and Jain, R.K. (1996). Transport in lymphatic capillaries. II. Microscopic velocity measurement with fluorescence photobleaching. Am. J. Physiol. *270*, H330–H337.

Bromley, S.K., Thomas, S.Y., and Luster, A.D. (2005). Chemokine receptor CCR7 guides T cell exit from peripheral tissues and entry into afferent lymphatics. Nat. Immunol. *6*, 895–901.

Bromley, S.K., Yan, S., Tomura, M., Kanagawa, O., and Luster, A.D. (2013). Recirculating memory T cells are a unique subset of CD4+ T cells with a distinct phenotype and migratory pattern. J. Immunol. *190*, 970–976.

Debes, G.F., Arnold, C.N., Young, A.J., Krautwald, S., Lipp, M., Hay, J.B., and Butcher, E.C. (2005). Chemokine receptor CCR7 required for T lymphocyte exit from peripheral tissues. Nat. Immunol. *6*, 889–894.

Dixon, J.B., Zawieja, D.C., Gashev, A.A., and Coté, G.L. (2005). Measuring microlymphatic flow using fast video microscopy. J. Biomed. Opt. *10*, 064016.

Förster, R., Schubel, A., Breitfeld, D., Kremmer, E., Renner-Müller, I., Wolf, E., and Lipp, M. (1999). CCR7 coordinates the primary immune response by establishing functional microenvironments in secondary lymphoid organs. Cell *99*, 23–33.

Förster, R., Braun, A., and Worbs, T. (2012). Lymph node homing of T cells and dendritic cells via afferent lymphatics. Trends Immunol. *33*, 271–280.

Geissmann, F., Cameron, T.O., Sidobre, S., Manlongat, N., Kronenberg, M., Briskin, M.J., Dustin, M.L., and Littman, D.R. (2005). Intravascular immune surveillance by CXCR6+ NKT cells patrolling liver sinusoids. PLoS Biol. *3*, e113.

Gunn, M.D., Kyuwa, S., Tam, C., Kakiuchi, T., Matsuzawa, A., Williams, L.T., and Nakano, H. (1999). Mice lacking expression of secondary lymphoid organ chemokine have defects in lymphocyte homing and dendritic cell localization. J. Exp. Med. *189*, 451–460.

Jat, P.S., Noble, M.D., Ataliotis, P., Tanaka, Y., Yannoutsos, N., Larsen, L., and Kioussis, D. (1991). Direct derivation of conditionally immortal cell lines from an H-2Kb-tsA58 transgenic mouse. Proc. Natl. Acad. Sci. USA *88*, 5096–5100.

Johnson, L.A., and Jackson, D.G. (2010). Inflammation-induced secretion of CCL21 in lymphatic endothelium is a key regulator of integrin-mediated dendritic cell transmigration. Int. Immunol. *22*, 839–849.

Kerjaschki, D., Regele, H.M., Moosberger, I., Nagy-Bojarski, K., Watschinger, B., Soleiman, A., Birner, P., Krieger, S., Hovorka, A., Silberhumer, G., et al. (2004). Lymphatic neoangiogenesis in human kidney transplants is associated with immunologically active lymphocytic infiltrates. J. Am. Soc. Nephrol. *15*, 603–612.

Kissenpfennig, A., Henri, S., Dubois, B., Laplace-Builhé, C., Perrin, P., Romani, N., Tripp, C.H., Douillard, P., Leserman, L., Kaiserlian, D., et al. (2005). Dynamics and function of Langerhans cells in vivo: dermal dendritic cells colonize lymph node areas distinct from slower migrating Langerhans cells. Immunity *22*, 643–654.

Lindquist, R.L., Shakhar, G., Dudziak, D., Wardemann, H., Eisenreich, T., Dustin, M.L., and Nussenzweig, M.C. (2004). Visualizing dendritic cell networks in vivo. Nat. Immunol. *5*, 1243–1250.

Luche, H., Weber, O., Nageswara Rao, T., Blum, C., and Fehling, H.J. (2007). Faithful activation of an extra-bright red fluorescent protein in "knock-in" Cre-reporter mice ideally suited for lineage tracing studies. Eur. J. Immunol. *37*, 43–53.

Lukas, M., Stössel, H., Hefel, L., Imamura, S., Fritsch, P., Sepp, N.T., Schuler, G., and Romani, N. (1996). Human cutaneous dendritic cells migrate through dermal lymphatic vessels in a skin organ culture model. J. Invest. Dermatol. *106*, 1293–1299.

Menning, A., Höpken, U.E., Siegmund, K., Lipp, M., Hamann, A., and Huehn, J. (2007). Distinctive role of CCR7 in migration and functional activity of naive- and effector/memory-like Treg subsets. Eur. J. Immunol. *37*, 1575–1583.

Moussion, C., and Girard, J.P. (2011). Dendritic cells control lymphocyte entry to lymph nodes through high endothelial venules. Nature *479*, 542–546.

Nitschké, M., Aebischer, D., Abadier, M., Haener, S., Lucic, M., Vigl, B., Luche, H., Fehling, H.J., Biehlmaier, O., Lyck, R., and Halin, C. (2012). Differential requirement for ROCK in dendritic cell migration within lymphatic capillaries in steady-state and inflammation. Blood *120*, 2249–2258.

Pflicke, H., and Sixt, M. (2009). Preformed portals facilitate dendritic cell entry into afferent lymphatic vessels. J. Exp. Med. *206*, 2925–2935.

Phillipson, M., Heit, B., Colarusso, P., Liu, L., Ballantyne, C.M., and Kubes, P. (2006). Intraluminal crawling of neutrophils to emigration sites: a molecularly distinct process from adhesion in the recruitment cascade. J. Exp. Med. *203*, 2569–2575.

Phillipson, M., Heit, B., Parsons, S.A., Petri, B., Mullaly, S.C., Colarusso, P., Gower, R.M., Neely, G., Simon, S.I., and Kubes, P. (2009). Vav1 is essential for mechanotactic crawling and migration of neutrophils out of the inflamed microvasculature. J. Immunol. *182*, 6870–6878.

Saeki, H., Moore, A.M., Brown, M.J., and Hwang, S.T. (1999). Cutting edge: secondary lymphoid-tissue chemokine (SLC) and CC chemokine receptor 7 (CCR7) participate in the emigration pathway of mature dendritic cells from the skin to regional lymph nodes. J. Immunol. *162*, 2472–2475.

Schumann, K., Lämmermann, T., Bruckner, M., Legler, D.F., Polleux, J., Spatz, J.P., Schuler, G., Förster, R., Lutz, M.B., Sorokin, L., and Sixt, M. (2010). Immobilized chemokine fields and soluble chemokine gradients cooperatively shape migration patterns of dendritic cells. Immunity *32*, 703–713.

Sen, D., Forrest, L., Kepler, T.B., Parker, I., and Cahalan, M.D. (2010). Selective and site-specific mobilization of dermal dendritic cells and Langerhans cells by Th1- and Th2-polarizing adjuvants. Proc. Natl. Acad. Sci. USA *107*, 8334–8339.

Stoitzner, P., Zanella, M., Ortner, U., Lukas, M., Tagwerker, A., Janke, K., Lutz, M.B., Schuler, G., Echtenacher, B., Ryffel, B., et al. (1999). Migration of langerhans cells and dermal dendritic cells in skin organ cultures: augmentation by TNF-alpha and IL-1beta. J. Leukoc. Biol. *66*, 462–470.

Swartz, M.A., Berk, D.A., and Jain, R.K. (1996). Transport in lymphatic capillaries. I. Macroscopic measurements using residence time distribution theory. Am. J. Physiol. *270*, H324–H329.

Tal, O., Lim, H.Y., Gurevich, I., Milo, I., Shipony, Z., Ng, L.G., Angeli, V., and Shakhar, G. (2011). DC mobilization from the skin requires docking to immobilized CCL21 on lymphatic endothelium and intralymphatic crawling. J. Exp. Med. *208*, 2141–2153.

Teijeira, A., Russo, E., and Halin, C. (2014). Taking the lymphatic route: dendritic cell migration to draining lymph nodes. Semin. Immunopathol. *36*, 261–274.

Ueno, H., Klechevsky, E., Morita, R., Aspord, C., Cao, T., Matsui, T., Di Pucchio, T., Connolly, J., Fay, J.W., Pascual, V., et al. (2007). Dendritic cell subsets in health and disease. Immunol. Rev. *219*, 118–142.

Ulvmar, M.H., Werth, K., Braun, A., Kelay, P., Hub, E., Eller, K., Chan, L., Lucas, B., Novitzky-Basso, I., Nakamura, K., et al. (2014). The atypical chemokine receptor CCRL1 shapes functional CCL21 gradients in lymph nodes. Nat. Immunol. *15*, 623–630.

Vigl, B., Aebischer, D., Nitschké, M., Iolyeva, M., Röthlin, T., Antsiferova, O., and Halin, C. (2011). Tissue inflammation modulates gene expression of lymphatic endothelial cells and dendritic cell migration in a stimulus-dependent manner. Blood *118*, 205–215.

Weber, M., Hauschild, R., Schwarz, J., Moussion, C., de Vries, I., Legler, D.F., Luther, S.A., Bollenbach, T., and Sixt, M. (2013). Interstitial dendritic cell guidance by haptotactic chemokine gradients. Science *339*, 328–332.

Wick, N., Haluza, D., Gurnhofer, E., Raab, I., Kasimir, M.T., Prinz, M., Steiner, C.W., Reinisch, C., Howorka, A., Giovanoli, P., et al. (2008). Lymphatic precollectors contain a novel, specialized subpopulation of podoplanin low, CCL27-expressing lymphatic endothelial cells. Am. J. Pathol. *173*, 1202–1209.

Yin, X., Johns, S.C., Kim, D., Mikulski, Z., Salanga, C.L., Handel, T.M., Macal, M., Zúñiga, E.I., and Fuster, M.M. (2014). Lymphatic specific disruption in the fine structure of heparan sulfate inhibits dendritic cell traffic and functional T cell responses in the lymph node. J. Immunol. *192*, 2133–2142.